Intermittency and the Talbot effect

Luis Vega

BCAM-UPV/EHU

Lyon, February 28, 2022

HADE

Outline

- The concepts
- Linear Schrödinger equation

$$\theta_M(x,t) = c_M \sum_k e^{iM^2tk^2+iMkx}$$

  - Gauss sums
  - Riemann's non differentiable function(**s**)

- Geometric point of view: Binormal flow (VFE)
- θ_M is a "solution" of 1d–NLS
- Transfer of energy
- Simplified model: α–Lévy processes

The **Talbot effect** is a near-field diffraction effect first observed in 1836 by Henry Fox Talbot. When a **plane wave** is incident upon a periodic **diffraction grating**, the image of the grating **is repeated at regular distances** away from the grating plane. The regular distance is called the **Talbot length**, and the repeated images are called self images or Talbot images. Furthermore, **at half the Talbot length**, a self-image also occurs, but **phase-shifted by half a period**. **At one quarter** of the Talbot length, the self-image is halved in size, and appears with **half the period of the grating (thus twice as many images are seen)**. At **one eighth** of the Talbot length, the period and size of the images is **halved again**, and so forth creating a **fractal pattern** of sub images with ever decreasing size, often referred to as a **Talbot carpet**.

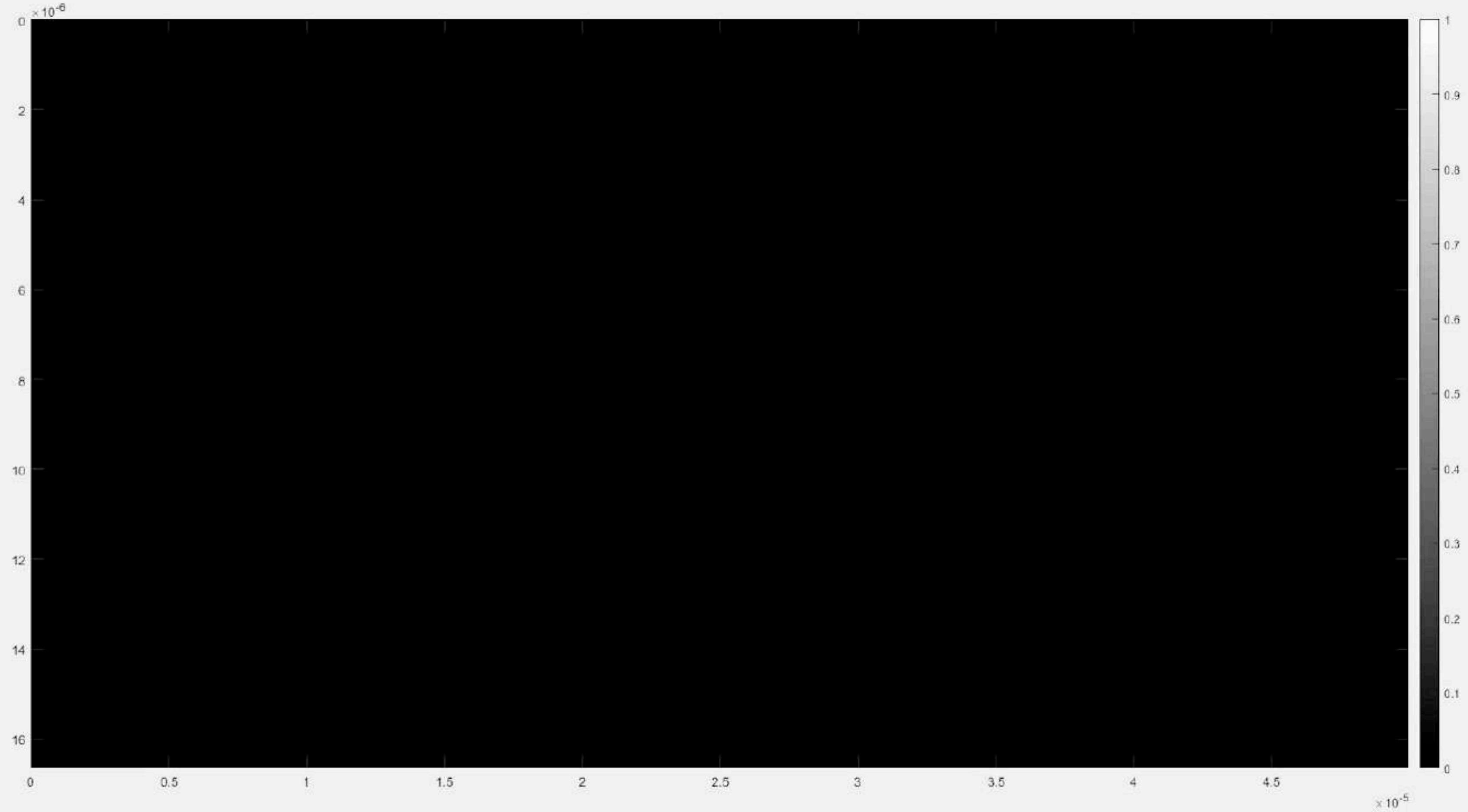
× 10-6
0
2
4
6
8
10
12
14
16
0
0.5
1
1.5
2
2.5
3
3.5
4
4.5
× 10-5
1
0.9
0.8
0.7
0.6
0.5
0.4
0.3
0.2
0.1
0

Intermittent behaviour is commonly observed in fluid flows that are **turbulent** or near the transition to turbulence. In highly **turbulent** flows, intermittency is seen in the irregular dissipation of kinetic energy [5] and the anomalous scaling of velocity increments.[6] It is also seen in the irregular alternation between turbulent and non-turbulent fluid that appear in turbulent **jets** and other turbulent free shear flows. In **pipe flow** and other wall bounded shear flows, there are intermittent puffs that are central to the process of transition from laminar to turbulent flow.

Intermittency has several meanings in turbulence. (One of them) is the tendency of the probability distributions of some quantities in three-dimensional Navier-Stokes turbulence, typically gradients or velocity differences, to develop long tails of very strong events. J Jiménez, 2006

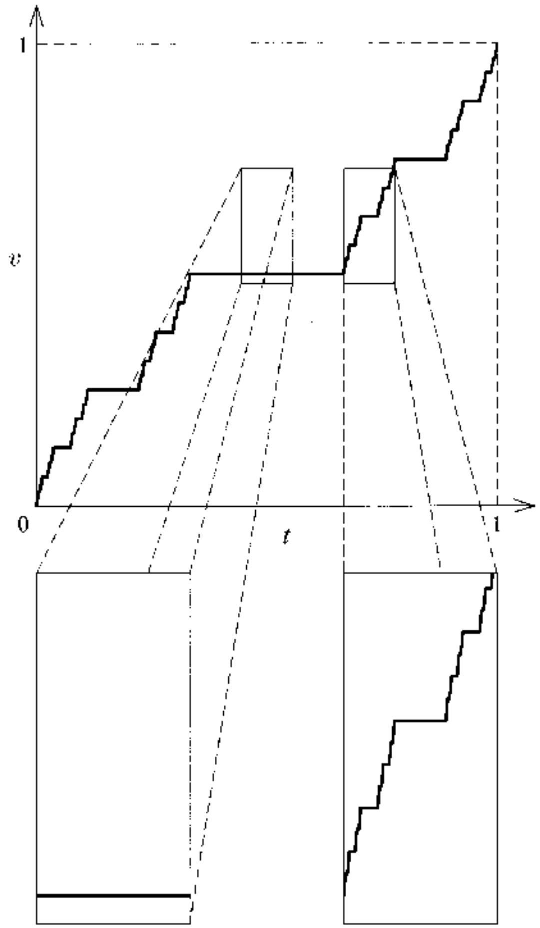

Fig. 8.2. The Devil's staircase: an intermittent function.

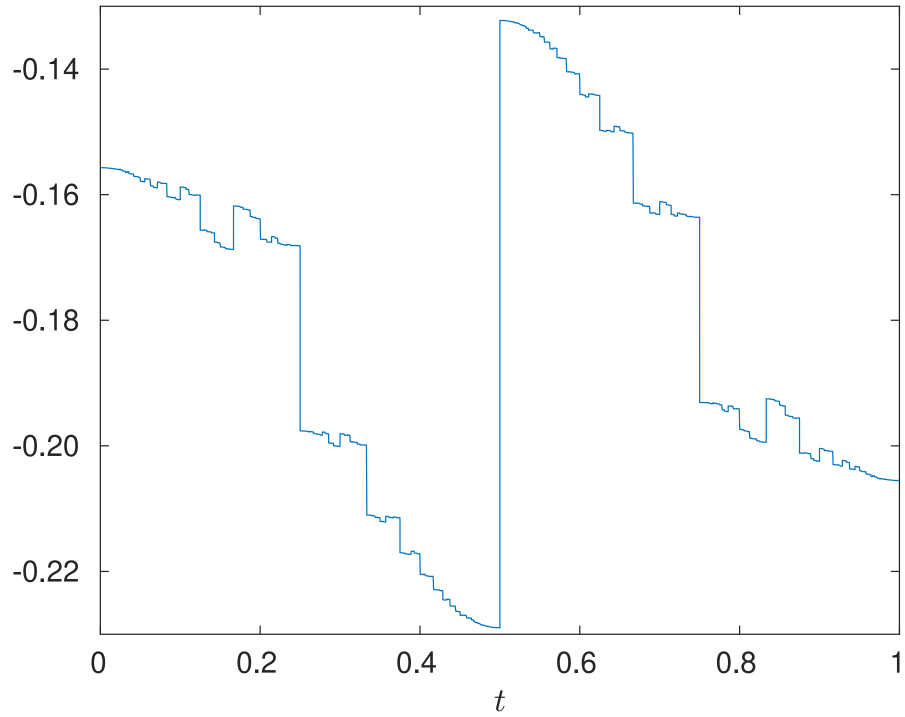

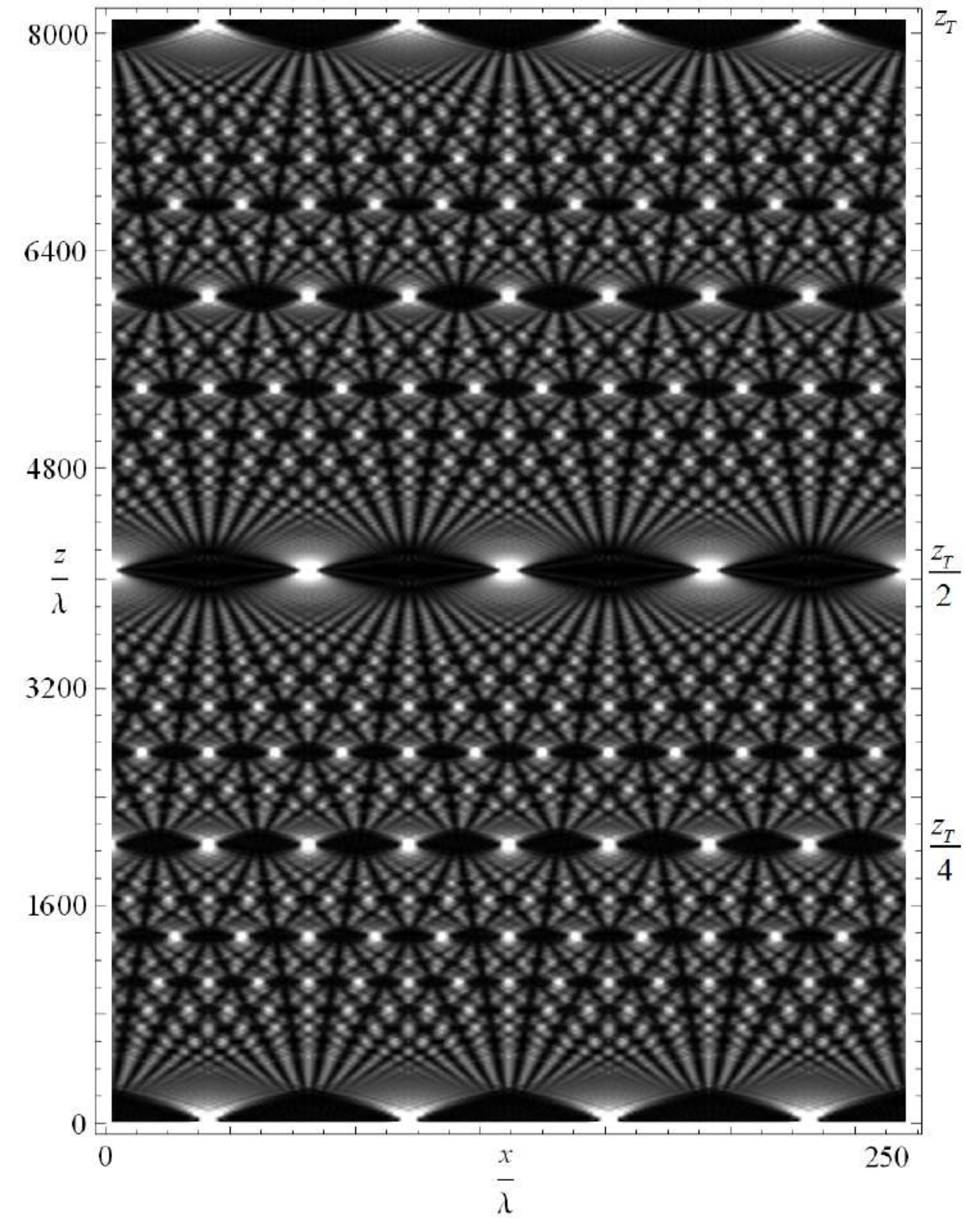

8000
6400
4800
3200
1600
0
$\frac{z}{\lambda}$
0
$\frac{x}{\lambda}$
250
z_T
$\frac{z_T}{2}$
$\frac{z_T}{4}$

Talbot effect and linear Schrödinger equation

$$\psi_t = i\psi_{xx}$$

$$\psi(x,0) = \frac{2\pi}{M} \sum_{k=-\infty}^{\infty} \delta\left(x - \frac{2\pi k}{M}\right)$$

$$\widehat{\psi}(k,t) = \frac{2\pi}{M} e^{-i(Mk)^2 t}$$

$$t_{pq} = (2\pi/M^2)(p/q)$$

$$\begin{aligned}
\theta_M(x, t_{pq}) := \psi(x, t_{pq}) &= \sum_{k=-\infty}^{\infty} e^{-i(Mk)^2 2\pi p/(M^2 q) + iMkx} \\
&= \sum_{k=-\infty}^{\infty} e^{-2\pi i(p/q)k^2 + iMkx} \\
&= \sum_{l=0}^{q-1} \sum_{k=-\infty}^{\infty} e^{-2\pi i(p/q)(qk+l)^2 + iM(qk+l)x} \\
&= \sum_{l=0}^{q-1} e^{-2\pi i(p/q)l^2 + iMlx} \sum_{k=-\infty}^{\infty} e^{iMqkx}.
\end{aligned}$$

The generalized quadratic Gauss sums are defined by

$$\sum_{l=o}^{|c|-1} e^{2\pi i(al^2+bl)/c},$$

for given integers a, b, c, with $c \neq 0$.

$$G(-p,m,q) = \begin{cases} \sqrt{q}e^{i\theta m}, & \text{if } q \text{ is odd,} \\ \sqrt{2q}e^{i\theta m}, & \text{if } q \text{ is even and } q/2 \equiv m \mod 2, \\ 0, & \text{if } q \text{ is even and } q/2 \not\equiv m \mod 2, \end{cases}$$

for a certain angle θ_m that depends on m (and, of course, on p and q, too).

The Talbot effect

$$t_{pq} = (2\pi/M^2)(p/q)$$

$$\theta_M(x,0) = \frac{2\pi}{M} \sum_{k=-\infty}^{\infty} \delta\left(x - \frac{2\pi k}{M}\right)$$

$$\theta_M(x,t_{pq}) = \frac{2\pi}{Mq} \sum_{k=-\infty}^{\infty} \sum_{m=0}^{q-1} G(-p,m,q)\delta\left(x - \frac{2\pi k}{M} - \frac{2\pi m}{Mq}\right)$$

$$\phi(t) = \sum_{k \neq 0} \frac{e^{\pi i k^2 t}}{i \pi k^2}, \quad t \in [0, 2]$$

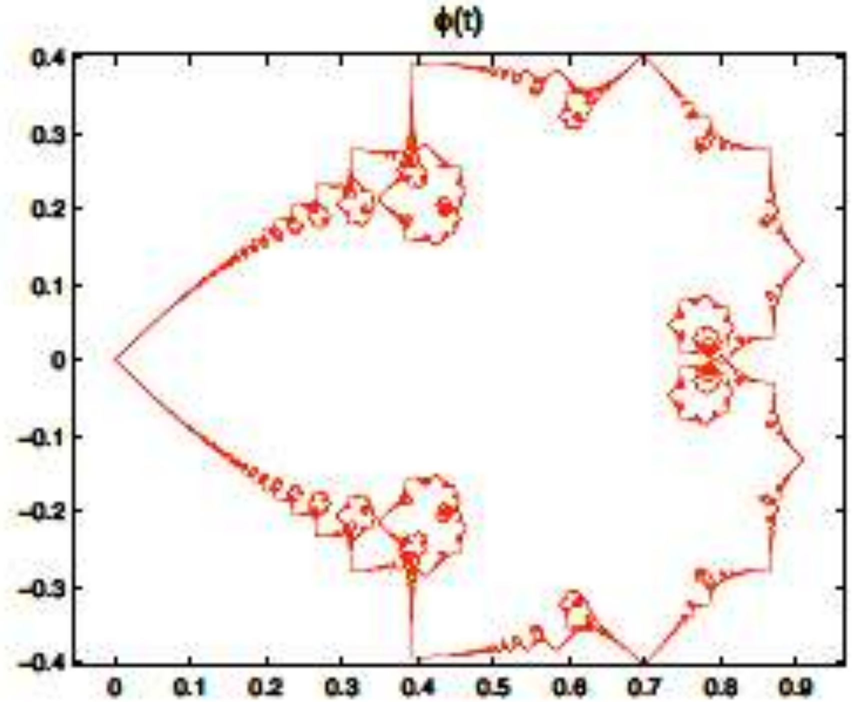

- Jaffard
- Multifractal (Frisch–Parisi conjecture)

Riemann's non–differentiable function

Integrating the Fourier series in time and evaluating at $x = 0$ we get

$$\phi(t) = i\int_0^t \theta_{2\pi}(0,\tau)d\tau = \sum_{k\in\mathbb{Z}} \frac{e^{-4\pi^2 ik^2 t} - 1}{-4\pi^2 k^2},$$

which is essentially Riemann's non–differentiable function.

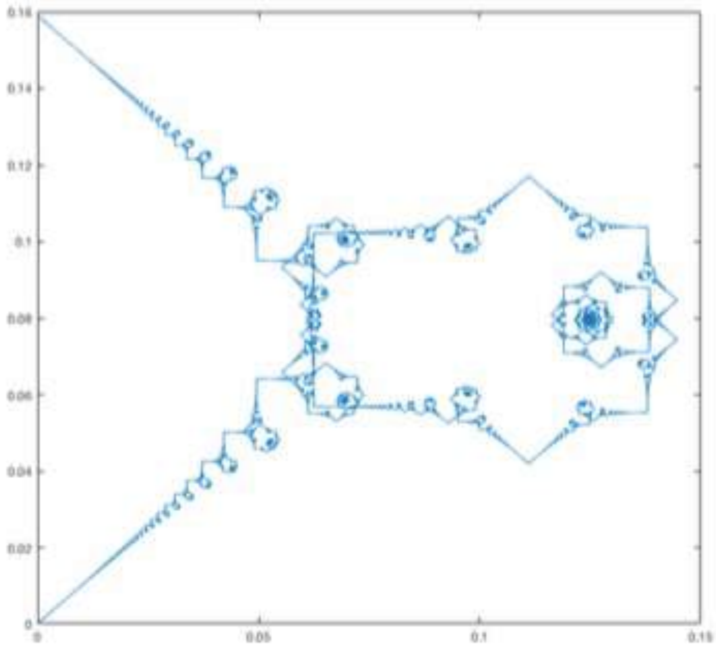

Figure: De la Hoz, Vega: *Vortex filament equation for a regular polygon*, Nonlinearity **27**(2014), 3031-3057

Annu. Rev. Fluid Mech. 1999. 31:239–72

FLOW CONTROL WITH NONCIRCULAR JETS[1]

E. J. Gutmark
Mechanical Engineering Department, Louisiana State University, Baton Rouge, Louisiana 70803-6413; e-mail: gutmark@me.lsu.edu

F. F. Grinstein
Laboratory for Computational Physics and Fluid Dynamics, Code 6410, Naval Research Laboratory, Washington, DC 20375-5344; e-mail: grinstei@lcp.nrl.navy.mil

KEY WORDS: vortices, mixing, combustion, entrainment

ABSTRACT

Noncircular jets have been the topic of extensive research in the last fifteen years. These jets were identified as an efficient technique of passive flow control that allows significant improvements of performance in various practical systems at a relatively low cost because noncircular jets rely solely on changes in the geometry of the nozzle. The applications of noncircular jets discussed in this review include improved large- and small-scale mixing in low- and high-speed flows, and enhanced combustor performance, by improving combustion efficiency, reducing combustion instabilities and undesired emissions. Additional applications include noise suppression, heat transfer, and thrust vector control (TVC).

The flow patterns associated with noncircular jets involve mechanisms of vortex evolution and interaction, flow instabilities, and fine-scale turbulence augmentation. Stability theory identified the effects of initial momentum thickness distribution, aspect ratio, and radius of curvature on the initial flow evolution. Experiments revealed complex vortex evolution and interaction related to self-induction and interaction between azimuthal and axial vortices, which lead to axis switching in the mean flow field. Numerical simulations described the details and clarified mechanisms of vorticity dynamics and effects of heat release and reaction on noncircular jet behavior.

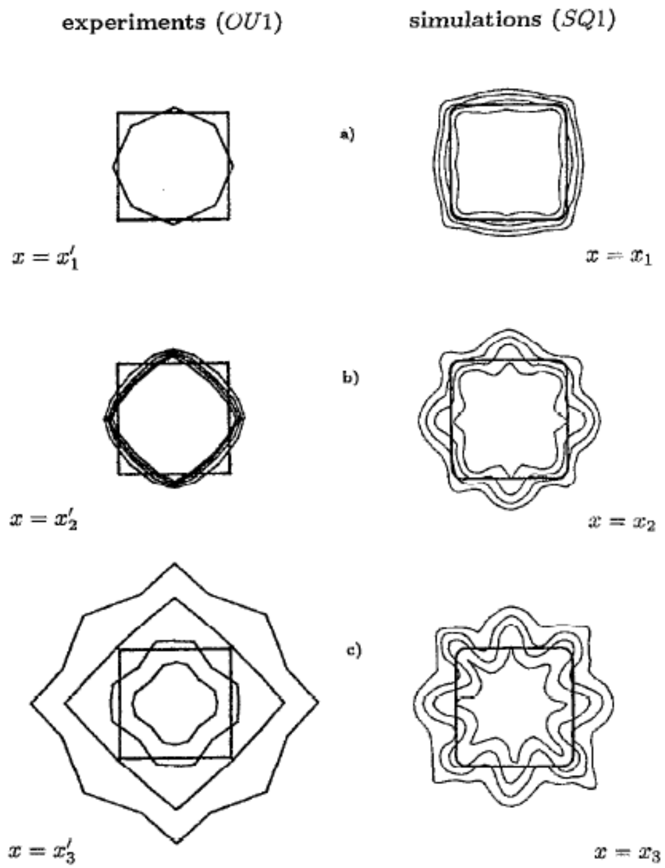

FIG. 10. Axis switching of the jet cross section in terms of isocontours of time-averaged streamwise velocity scaled with its local centerline value

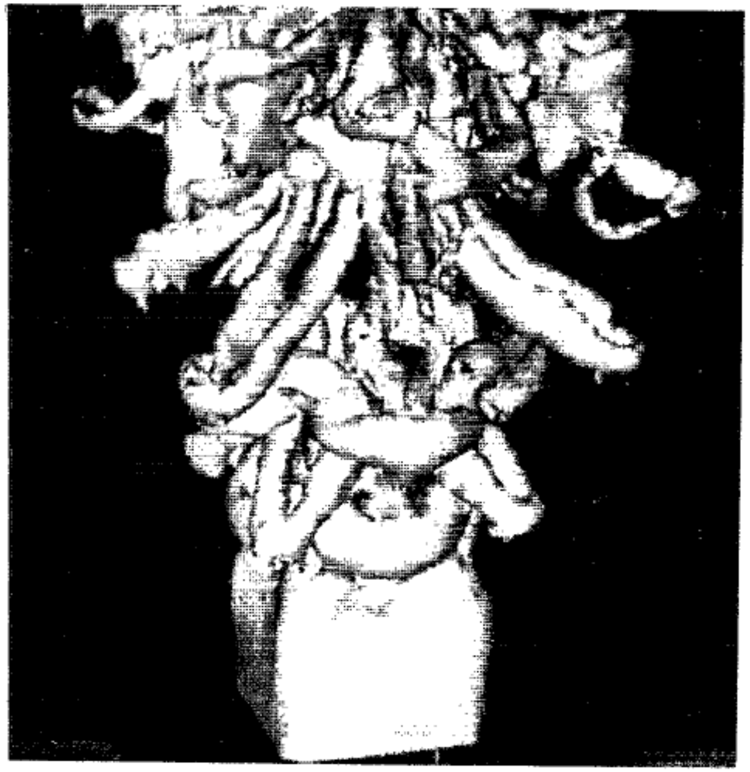

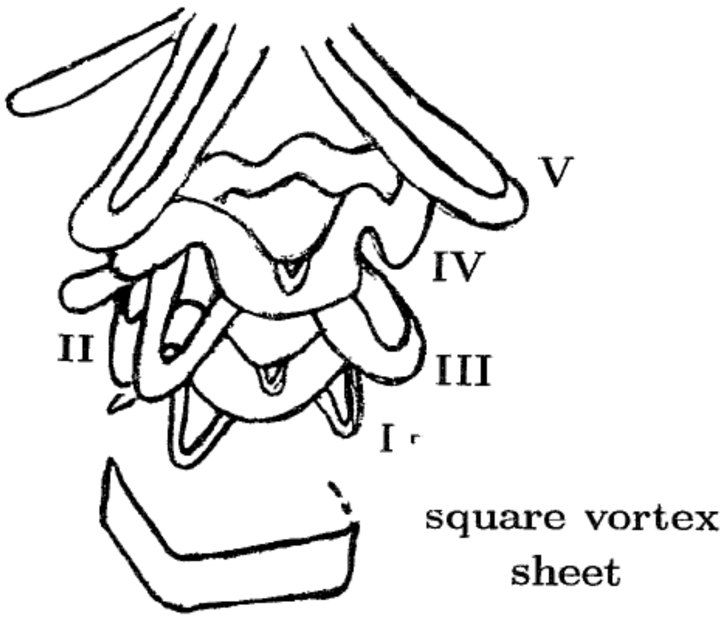
I, III, V : hairpin (braid) vortices
II, IV : deformed vortex rings
V
IV
II
III
I
square vortex
sheet

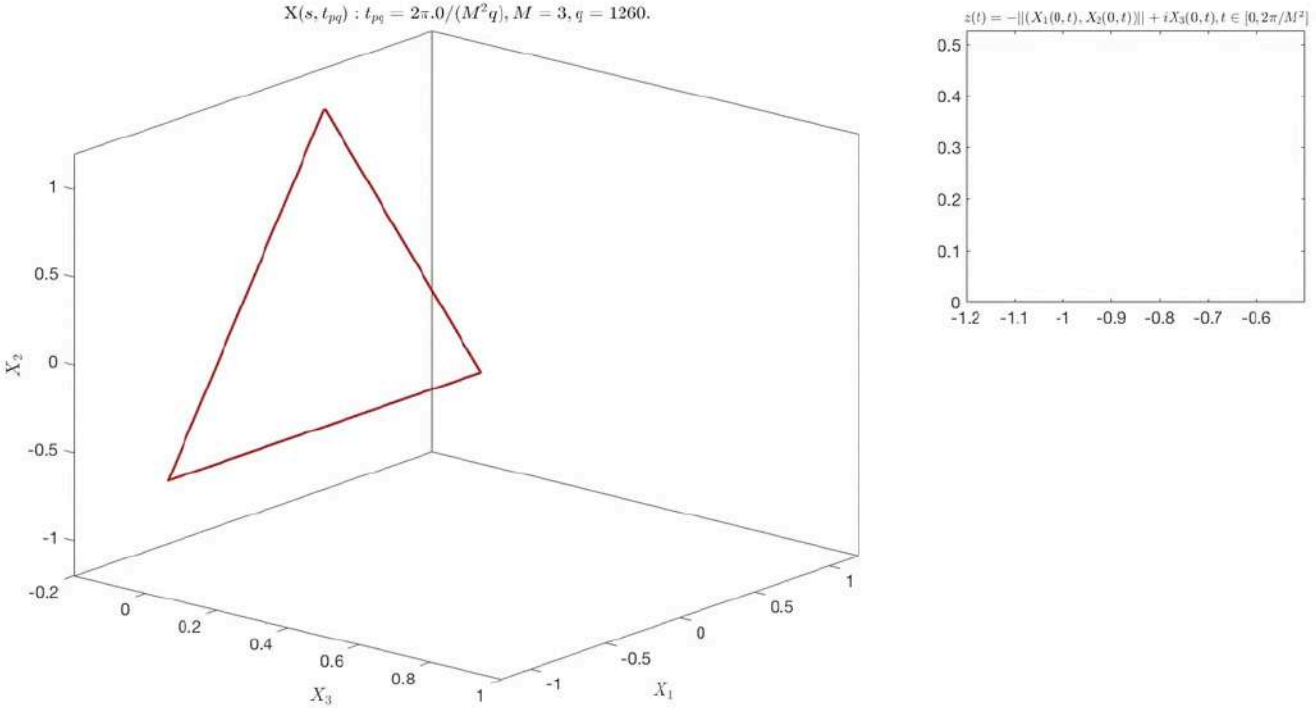

X(s, t_{pq}) : $t_{pq} = 2\pi.0/(M^2 q), M = 3, q = 1260.$
X_2
X_3
X_1
$z(t) = -||(X_1(0,t), X_2(0,t))|| + iX_3(0,t), t \in [0, 2\pi/M^2]$

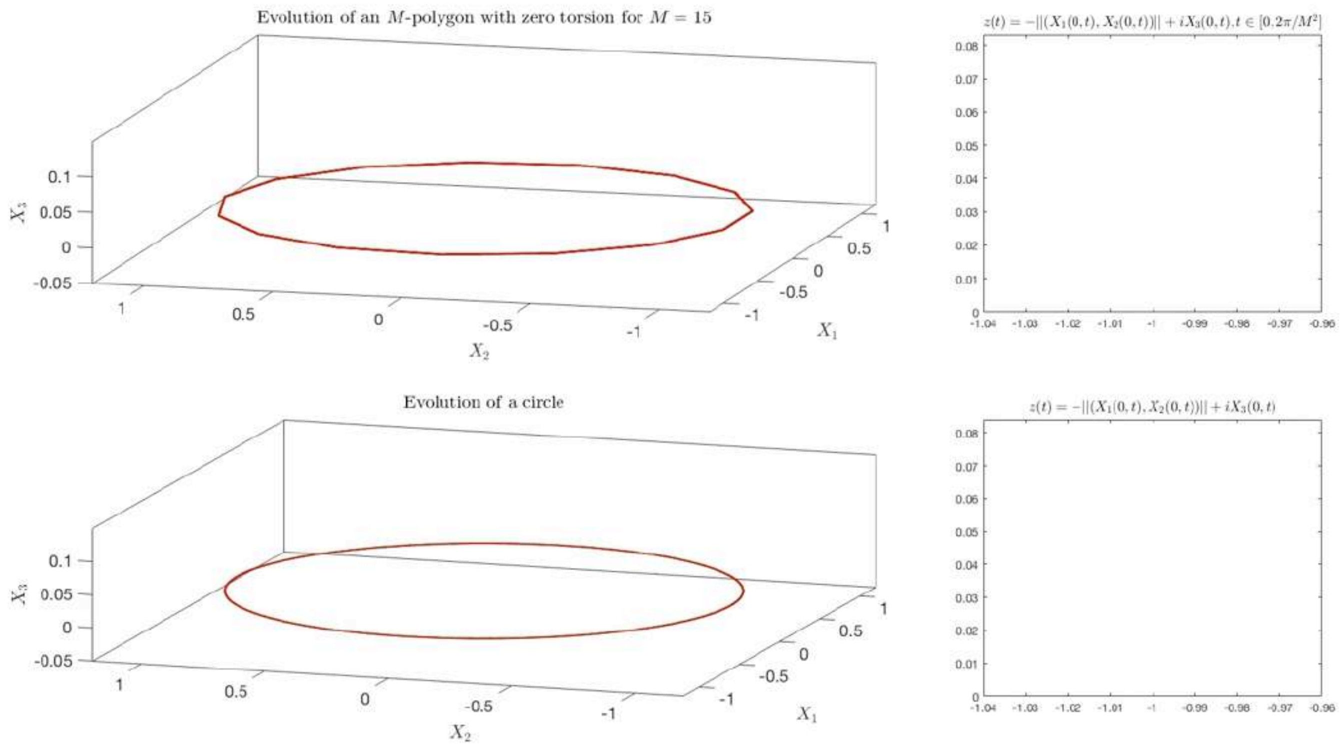

Evolution of an M-polygon with zero torsion for $M = 15$
X_3
0.1
0.05
0
-0.05
1
0.5
0
-0.5
-1
X_2
X_1
$z(t) = -||(X_1(0,t), X_2(0,t))|| + iX_3(0,t), t \in [0, 2\pi/M^2]$
0.08
0.07
0.06
0.05
0.04
0.03
0.02
0.01
-1.04
-1.03
-1.02
-1.01
-1
-0.99
-0.98
-0.97
-0.96
Evolution of a circle
$z(t) = -||(X_1(0,t), X_2(0,t))|| + iX_3(0,t)$

Binormal flow

(BF) • $\chi_t = \chi_x \wedge \chi_{xx} = cb \quad c : \text{curvature} \quad b : \text{binormal}$

(SM) • $\chi_x = T$ Schrödinger map $\qquad T_t = T \wedge T_{xx}$

(NLS) • u Hasimoto wave function 1d **NLS** (cubic focusing)

$$\chi(0,x) : \quad \text{skew polygonal line}$$

$$T(0,x) : \quad \text{sequence of points } T_j \text{ such that } \lim_{j\to\pm\infty} T_j = A^{\pm}$$

$$u(0,x) = \sum a_j \delta(x-j) \qquad \sum_j |j|^{1^+} |a_j|^2 < +\infty$$

We consider the IVP

$$\partial_t u = i\left(\partial_x^2 u + \left(|u|^2 - M(t)\right)u\right) \qquad M(t) \in \mathbb{R}$$
$$u(x,0) = u_0(x) \qquad x \in \mathbb{R}$$

- **Hasimoto transformation:**

$$\begin{pmatrix} T \\ e_1 \\ e_2 \end{pmatrix}_x = \begin{pmatrix} 0 & \alpha & \beta \\ -\alpha & 0 & 0 \\ -\beta & 0 & 0 \end{pmatrix} \begin{pmatrix} T \\ e_1 \\ e_2 \end{pmatrix}$$

$$u = \alpha + i\beta$$

$$u = \rho e^{i\phi} \qquad \rho : \text{ curvature} \qquad \nabla\phi = \text{ torsion}$$

$$u(x,t) = c_M \sum_k e^{itk^2+ikx}$$

- It is a "solution" of 1d–cubic NLS **(NLS)**
- It has a geometrical meaning:

  Binormal Flow **(BF)**

  Schrödinger map **(SM)**

- (NL) Talbot effect:
  - Intermittency
  - Multifractality

Theorem **(BV 2021)**

Assume

$$\begin{cases} a_{-1} = a = a_{+1} & a \neq 0 \\ a_j = 0 & \text{otherwise} \end{cases}$$

Then there exists $c > 0$

$$\sup_{\xi} \left| \widehat{T_x}(\xi, t) \right|^2 \geq c |\lg t| \qquad t > 0.$$

- **Colliander, Keel, Staffilani, Takaoka, Tao 2010**
- **Hani, Pausader, Tzvetkov,Visciglia 2015**

- This cascade can be understood associated to a linear problem.

$$(T, e_1, e_2) \quad \text{orthonormal frame}$$

$$\begin{aligned} T_x &= \alpha e_1 + \beta e_2 \\ e_{1x} &= -\alpha T \\ e_{2x} &= -\beta T \end{aligned}$$

$$\begin{aligned} T_t &= -\beta_x e_1 + \alpha_x e_2 \\ e_{1t} &= -\alpha_x T + (|u|^2 - M(t)) e_2 \\ e_{2t} &= -\beta_x T - (|u|^2 - M(t)) e_1 \end{aligned}$$

$$\alpha + i\beta = \frac{1}{\sqrt{t}} e^{i\frac{|x|^2}{4t}} \overline{V}\left(\frac{x}{2t}, \frac{1}{t}\right) = u(x,t)$$

$$\alpha_x + i\beta_x = u_x = i\frac{x}{2t}u + \text{“small”}$$

(Chevillard et al. 2021)

- This cascade can be understood associated to a linear problem.

$$(T, e_1, e_2) \quad \text{orthonormal frame}$$

$$\begin{aligned} T_x &= \alpha e_1 + \beta e_2 \\ e_{1x} &= -\alpha T \\ e_{2x} &= -\beta T \end{aligned}$$

$$\begin{aligned} T_t &= -\beta_x e_1 + \alpha_x e_2 \\ e_{1t} &= -\alpha_x T + (|u|^2 - M(t)) e_2 \\ e_{2t} &= -\beta_x T - (|u|^2 - M(t)) e_1 \end{aligned}$$

$$\alpha + i\beta = u(x,t) = c_M \sum_{k=-\infty}^{\infty} e^{-iM^2 t k^2 + iMkx}$$

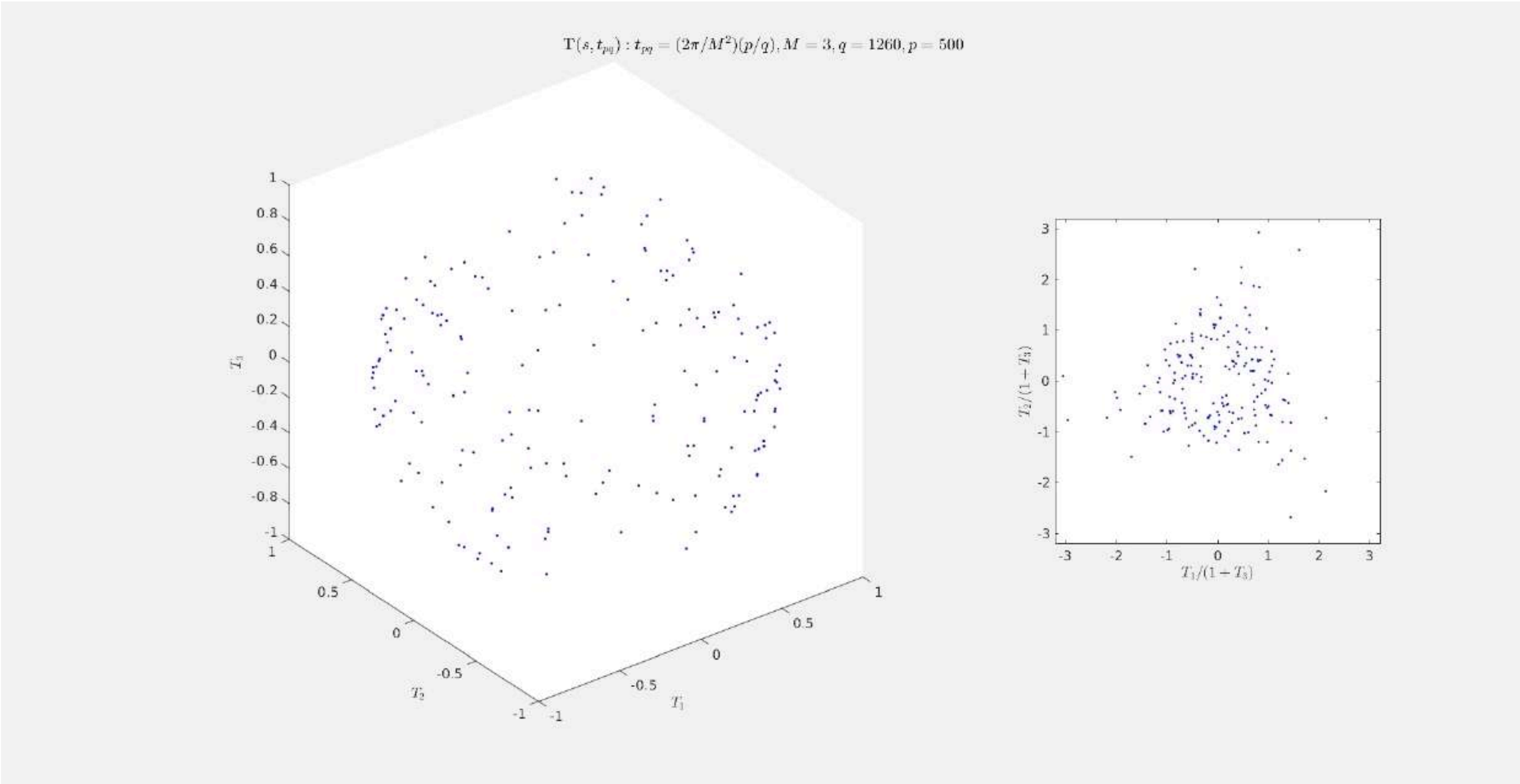

$\mathrm{T}(s, t_{pq}) : t_{pq} = (2\pi/M^2)(p/q), M = 3, q = 1260, p = 500$
T_3
T_2
T_1
$T_2/(1-T_3)$
$T_1/(1-T_3)$

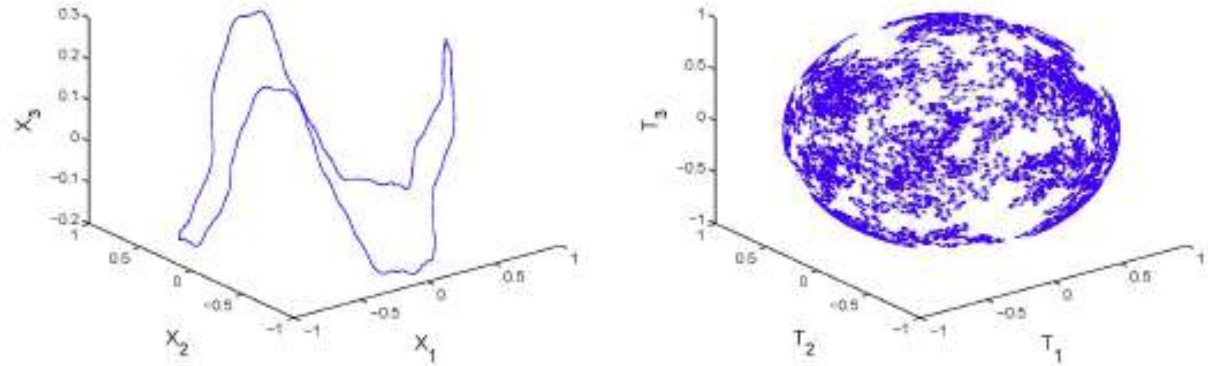

Figure 8: $\mathbf{X}_{alg}$ and $\mathbf{T}_{alg}$, at $t = \frac{2\pi}{9}(\frac{1}{4} + \frac{1}{41} + \frac{1}{401}) = \frac{2\pi}{9} \cdot \frac{18209}{65764}$.

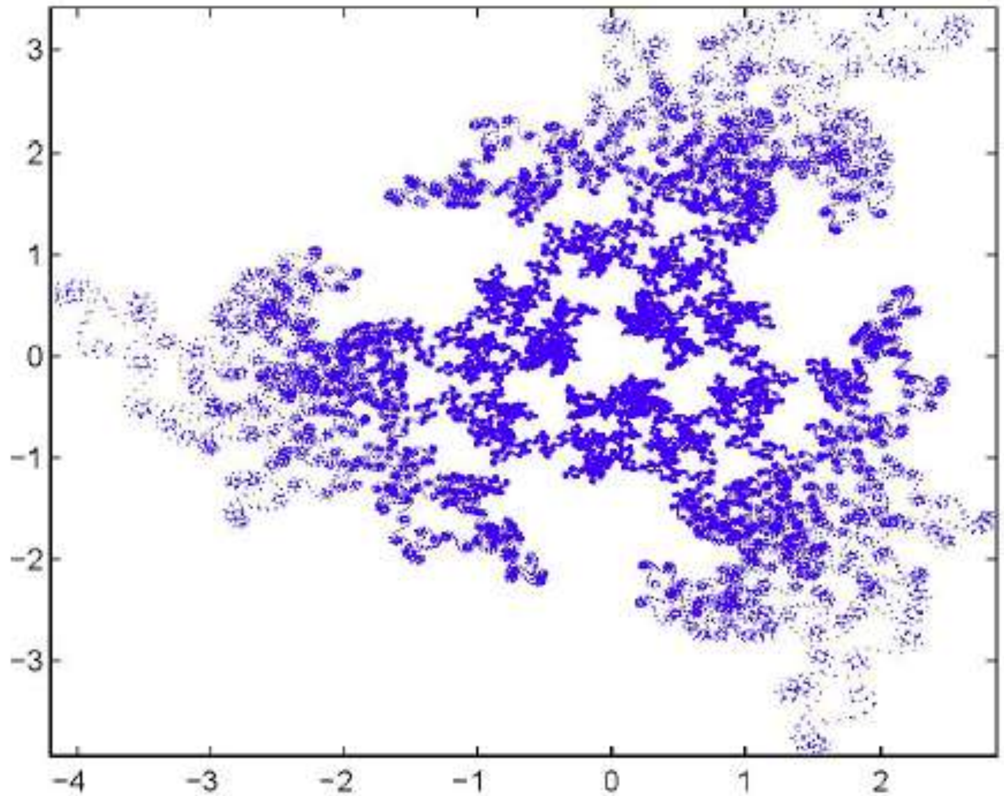

Figure 9: Stereographic projection of the right-hand side of Figure 8.

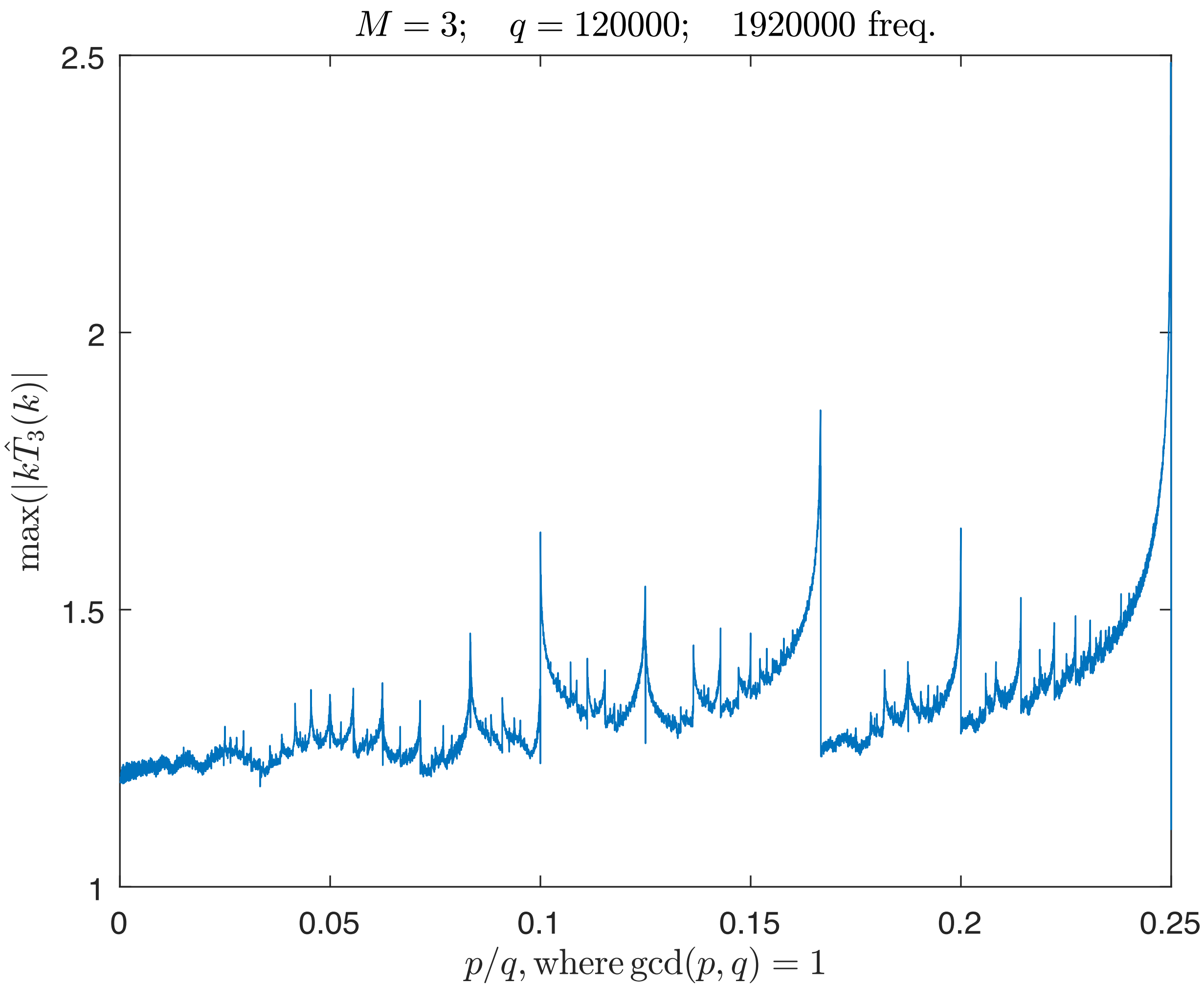
$M = 3$; $q = 120000$; 1920000 freq.
2.5
2
1.5
1
0
0.05
0.1
0.15
0.2
0.25
$\max(|k\hat{T}_3(k)|)$
p/q, where $\gcd(p,q) = 1$

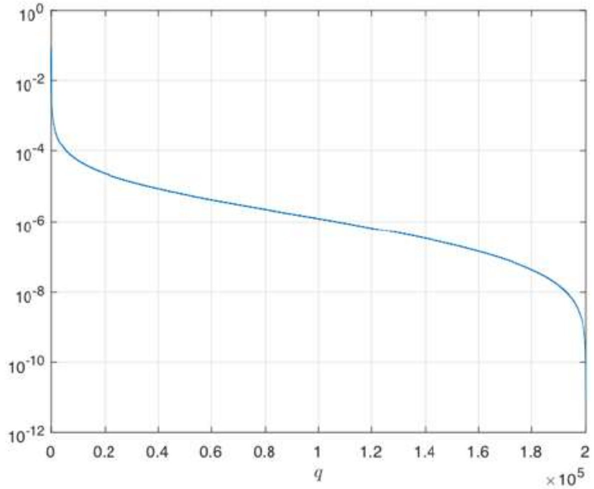

Figure 10: $|\sqrt{2}\max_{t_{pq}} \|\widehat{T_{1,s}}(t_{pq})\|_\infty - a\ln(q) - b|$, for $a = 0.258039752572419$, $b = 0.152992510344641$.

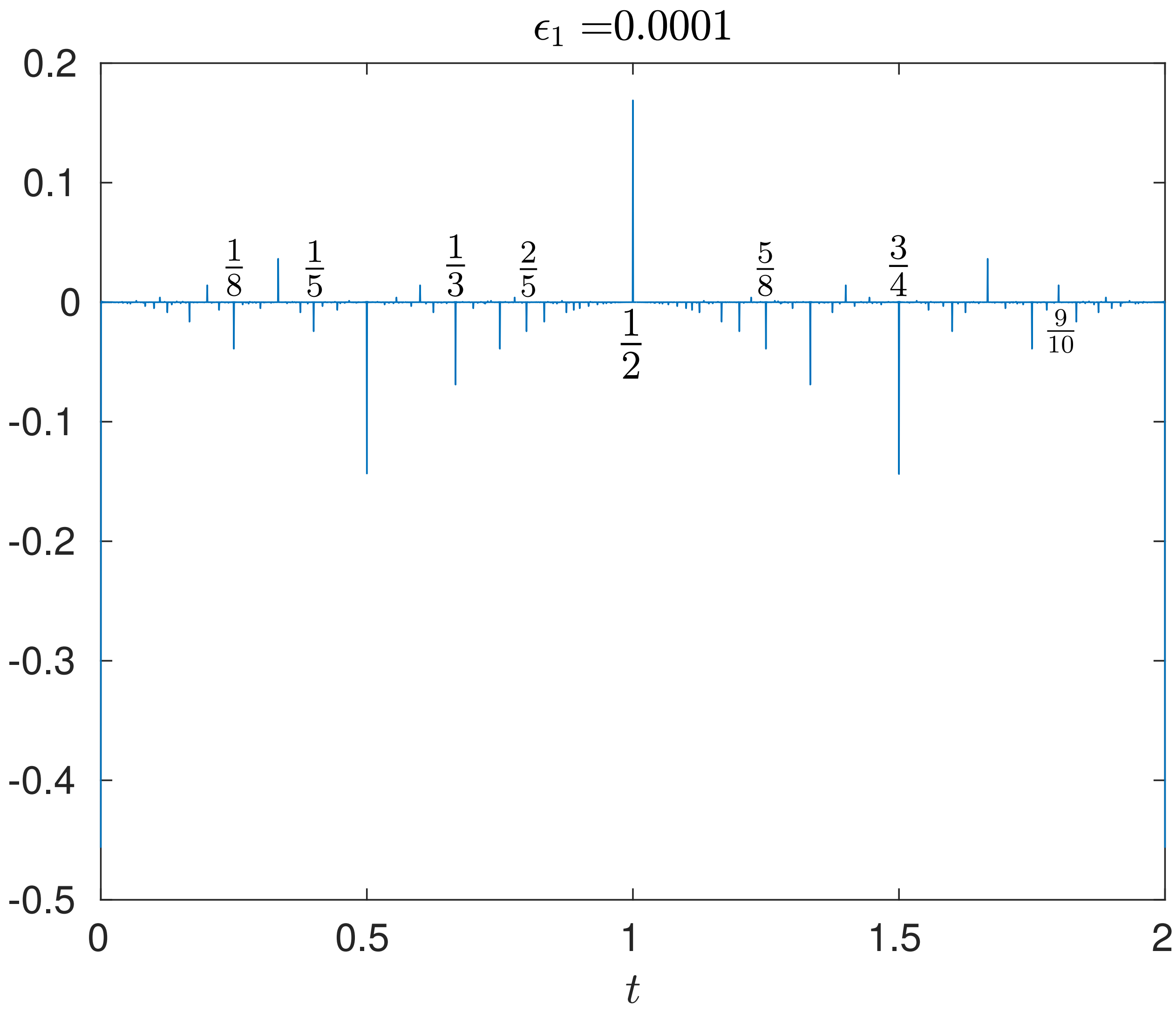

Figure 2: Plot of $h_{\mathrm{p},\delta}[F_{\varepsilon_1}]$ when $\delta = 0.25$.

$$H_\delta(t) := \int_{[0,t]} h_{\mathrm{p},\delta}(2s)ds.$$

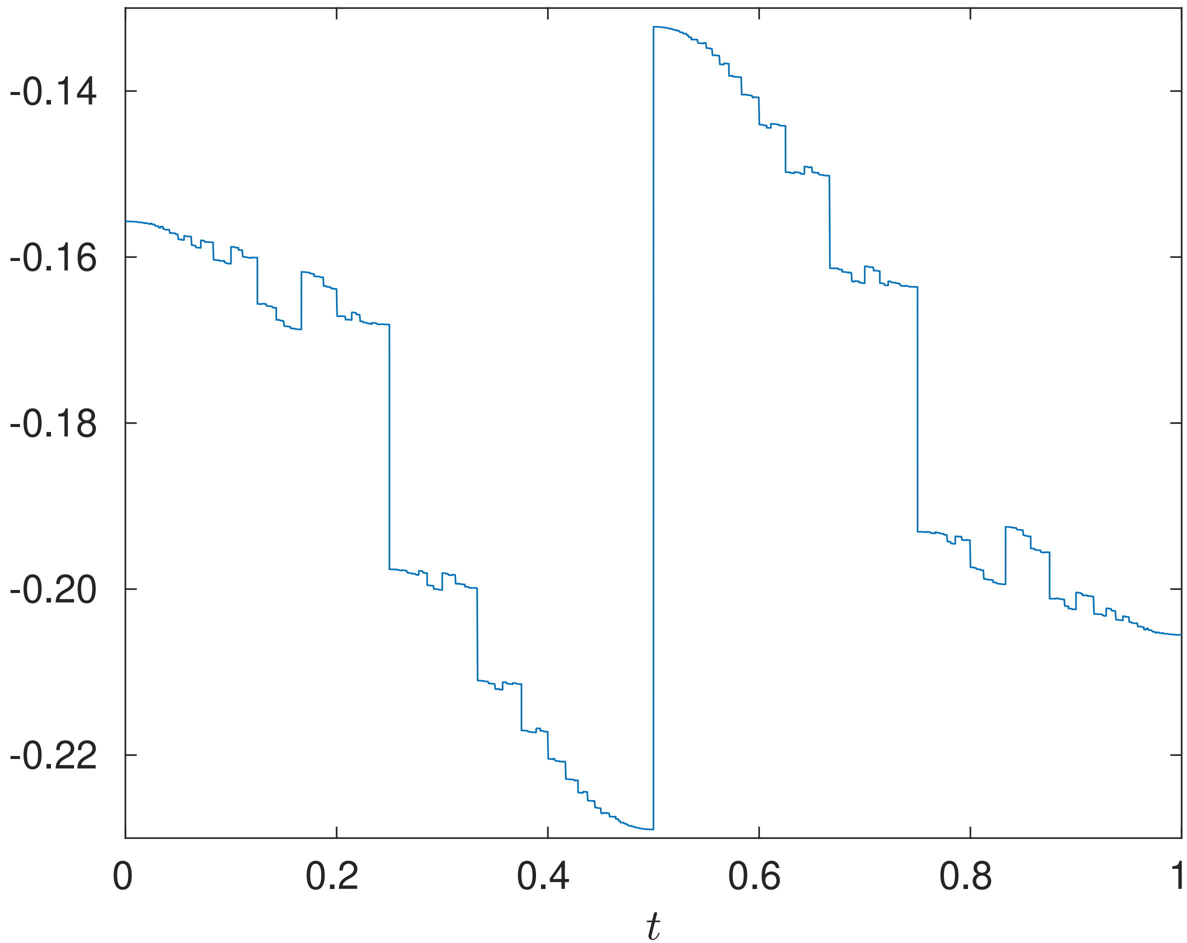

Figure 3: Plot of H_δ. Even though H_δ has some symmetry, *e.g.* $H_\delta(1-t) = c_\delta - H_\delta(t-)$, the appearance of "unpredictable" large jumps resembles an α-Lèvy process with small exponent α.

THANK YOU FOR YOUR ATTENTION